Synthesis and characterization of Mg–Co catalytic oxide materials for low-temperature N_2O decomposition

Min Qian and Hua C. Zeng*

Department of Chemical Engineering, Faculty of Engineering, National University of Singapore, 10 Kent Ridge Crescent, Singapore 119260

Binary metal Mg–Co oxide materials have been synthesized from Mg–Co hydroxide precursors by a coprecipitation-then-calcination method. The oxide system shows high catalytic activity for low-temperature decomposition of N_2O (27 mol%). Using FTIR, XRD, SEM, EA, DSC, BET and GC techniques, the hydrothermal synthesis and chemistry of the double-metal hydroxides have been studied in detail. In anion exchange and XRD studies, a hydrotalcite-like phase is also found to be present in the hydroxides owing to a partial oxidation of Co^{2+} to Co^{3+} in air. The precursor subjected to hydrothermal treatment has a higher Mg content, higher crystallinity and is more stable compared to the one aged at room temperature. However, they all give amorphous Mg–Co oxides after calcination. The Mg–Co oxide prepared from the hydrothermally treated precursor has a higher surface area and is more active for N_2O decomposition. With this material system, *ca.* 6 moles of N_2O per kg of the precursor materials can be decomposed at 350 °C within 1 h.

Recently, catalytic decomposition of nitrous oxide (N_2O) has become an important sub-field of de-NO_x research,[1–18] owing to the increasing concern about the earth's atmospheric control. N_2O is generally considered as a greenhouse gas, because it is 320 times as effective in capturing atmospheric heat as an equal volume of carbon dioxide. Furthermore, N_2O gas also contributes to catalytic stratospheric ozone destruction. Industrial emissions of N_2O are increasing mainly from the use of circulating fluidized beds for combustion, automotive exhaust emission, nitric acid production and the global manufacture of large amount of adipic acid for nylon-66.[1,2,4] Besides these chemical processes, agricultural sources due to anthropogenic nitrogen fixation also make a noticeable contribution to the overall increase in atmospheric N_2O.[3] As far as the above sources are concerned, the N_2O concentration ranges from several hundred ppm in a fluidized bed combustion of coals (< 500 ppm) to a few tens of mol% in a gas stream of adipic acid manufacturing.[4,11]

To tackle increasing N_2O emissions, a great variety of catalytic materials and processes have been developed over the last 10–15 years.[1–18] Very recently, new oxide catalysts prepared from the thermal decomposition of hydrotalcite-like compounds (HTlc), M-Al-CO_3-HT (M = Ni, Co, Cu), have shown high catalytic activities in low-temperature N_2O decomposition,[17] where the catalyst can be operated at a temperature as low as 150–400 °C. This class of materials promises a new generation of catalysts for future low-temperature N_2O decomposition. Chemically, the HTlc precursors[19,20] of the above catalysts are the mixed-metal hydroxides with oxidation state 2+ for transition metals and 3+ for Al. It is believed that the catalytic activity achieved is due to a correct combination of the chemical composition, oxidation states of the metals and the structural properties of the precursor materials.

In the hydrotalcite compound, Mg-Al-CO_3-HT, both divalent Mg^{2+} and trivalent Al^{3+} cation elements are located in brucite sheets while the anion species (CO_3^{2-}) is in the inter-sheet space.[21] Likewise, the above-mentioned HTlc materials have a similar structure, except that the alkaline-earth-metal Mg^{2+} in the brucite sheets is now substituted by the divalent transition-metal cations.[17] From the materials viewpoint, it would be of interest to explore the catalytic activity of the calcined HTlc materials when the trivalent Al^{3+} is replaced by transition metals, instead of Mg^{2+}. Materials chemistry studies on these layered materials, including on other intercalation compounds, will help us to design and develop active catalysts, since the precursor materials determine the ultimate performance of the catalyst.

In this paper, we report a systematic study on another type of double-metal (Mg–Co) hydroxide/hydrotalcite precursor for low-temperature N_2O decomposition. The study also looks into the chemical composition, anion exchangeability, surface morphology, and chemical and thermal stabilities of these non-Al-containing materials upon hydrothermal processing. It is important to mention that, unlike most N_2O decomposition studies carried out at low concentrations of a few hundred ppm, the current work used a concentrated N_2O gas (27 mol%) to account for the off-gas stream of adipic acid production.

Experimental

Materials preparation

Double-metal hydroxides of Mg–Co were prepared using the coprecipitation method. Briefly, a 60 ml mixed aqueous nitrate solution of Mg–Co (total cation concentration = 1.0 mol dm^{-3}; $Mg(NO_3)_2 \cdot 6H_2O$, > 99.0%, Merck; $Co(NO_3)_2 \cdot 6H_2O$, > 99.0%, Fluka) with a molar ratio of 1:1 was added to 300 ml of a 0.5 mol dm^{-3} ammonia solution (pH = 9.5) in a 500 ml two-necked round-bottomed flask. The addition of metal cations was carried out under stirring at room temperature, after which, the flask was sealed to prevent inter-diffusion between ambient air and water and ammonia vapours in the reaction flask.

Two types of ageing treatment were then performed. (i) The above-prepared precipitate (MC; M = Mg, C = Co) in the sealed flask was stirred at room temperature for another 5 h, followed by filtering and washing with deionized water. The resultant precipitate was then dried in air at 60 °C overnight (18 h); the sample is referred to hereafter as MC1. (ii) The precipitate (MC) was treated hydrothermally at 65 °C for 18 h with continuous stirring. Filtering, washing and drying (60 °C, overnight) then gave a sample referred to hereafter as MC2.

The final pH value for the system was *ca.* 9.0 after the above ageing treatments. In the thermal stability study, the above-prepared MC1 and MC2 samples were further heat-treated at 150, 200, 250, 300 and 350 °C, respectively, for 2 h with static air in an electric furnace (Carbolite).

The anion-exchange properties of the MC1 and MC2 samples were investigated using the impregnation method. This involved impregnating the finely ground MC1 and MC2 powders in a sodium carbonate solution (0.5 mol dm^{-3}, Na_2CO_3, 99.9%, BDH) for different times (5 min to 10 h) under magnetic stirring at room temperature. Filtering, washing and drying (details as above) were then carried out for these CO_3^{2-}-treated materials.

To conduct comparative studies, pure forms of the monohydroxides of Mg and Co were also prepared using the procedure described above. The cation solutions for Mg and Co were 1.0 mol dm^{-3} in these cases; the other parameters and treatments were unaltered.

Materials characterization

Crystallographic details for the prepared materials were established using the X-ray diffraction (XRD) method. The diffraction intensity *vs.* 2θ spectra were measured in a Philips PW 1729 instrument with Cu-Kα radiation ($\lambda = 1.5418$ Å) with a 2θ range of 5–70° at a scanning rate of 4° min^{-1}. The crystallinity and morphology of the samples were examined by scanning electron microscopy (SEM, JEOL JSM-T330A). To improve the electric conductivity, the samples were surface-coated with a gold layer of thickness *ca.* 10 nm in a vacuum evaporator (JEOL-JEE-4X) prior to the SEM analyses.

The chemical compositions of the as-prepared and CO_3^{2-}-treated samples were investigated with elemental analysis (EA) in a Labtam Plasmascan F10 instrument using inductively coupled plasma–atomic emission spectroscopy. Metal–oxygen bonds and included functional groups (anions) were studied by FTIR spectroscopy (Shimadzu FTIR-8101) using the potassium bromide (KBr) pellet technique. Forty scans were performed for each spectrum to ensure a good signal to noise ratio.

To investigate the thermal behaviour of the above materials, differential scanning calorimetry (DSC, Netzsch DSC200) studies were conducted. Samples for DSC measurements were heated from 40 to 500 °C at a rate of 10 °C min^{-1} under a nitrogen atmosphere with a gas flow-rate of 15 ml min^{-1}. Surface areas of the heat-treated samples were determined by N_2 adsorption–desorption in a NOVA1000 instrument, using the BET equation. Prior to the BET measurement, each calcined sample received a degas treatment under vacuum for 1 h at a temperature lower than the calcination temperature used.

Catalytic activity evaluation

For catalytic activity evaluation, the as-prepared MC1 and MC2 powders were vacuum-pressed under an external pressure of 6 tonnes cm^{-2}. The pressed MC1 and MC2 plates were then divided and screened with sizes of 355 to 1000 μm.

The catalytic activities of MC1 and MC2 were evaluated in a quartz-tube microreactor with a constant diameter of 1.0 cm. The above-prepared MC1 and MC2 (mass 0.605 g, volume, V 0.5×10^{-3} dm^3) were added to the quartz reactor. Prior to the catalytic test the MC1 or MC2 was decomposed *in situ* under an N_2O–He flow at 350 °C. After the above heat-treatment, MC1 and MC2 had been converted to metal oxides owing to the depletion of OH groups. The N_2O decomposition experiment was then carried out on the resulting oxide catalyst. In these experiments, the N_2O gas was supplied continuously from a gas cylinder (27 mol% N_2O + 73 mol% He) at a flow-rate (F) of 1.5 dm^3 h^{-1} and the GHSV (F/V) for the feed gas thus corresponds to 3000 h^{-1}. The decomposed gases were cooled in a cooling coil and then vented through a scrubber. The inlet and outlet gas compositions were analysed by gas chromatography on a Shimadzu GC-14A (TCD detector) using a Porapak Q column (4 m length) with He as the carrier gas (20 ml min^{-1}). Other experimental arrangements have been described in detail in our previous publications.[4,18]

The catalyst activity was evaluated in terms of the conversion rate (X) of the N_2O gas.[18] N_2O decomposition is a mole-number-increasing reaction ($N_2 + 1/2\ O_2$). Eqn. (1) considers this fact and has been used in evaluation of catalytic activity of N_2O decomposition,[18] noting that the partial pressures have the same values as their respective molar fractions since the total pressure is 1 atm:

$$X = (p_{in,N_2O} - p_{out,N_2O})/(p_{in,N_2O} + 0.5 p_{in,N_2O} p_{out,N_2O}) \quad (1)$$

where p_{in,N_2O} and p_{out,N_2O} are the partial pressures of N_2O in the inlet and outlet gases respectively.

Results and Discussion

Formation of double-hydroxide compounds

Fig. 1 displays the FTIR spectra of the as-prepared MC1 and MC2, along with those of the monohydroxides $Mg(OH)_2$ and $Co(OH)_2$. In all samples, the sharp strong peaks located at 3700–3631 cm^{-1} are assigned to OH vibrations of the metal hydroxides whereas the broad absorption bands at 3434–3488 cm^{-1} can be attributed to OH vibrational modes of water molecules which are inter-connected with other H_2O molecules and with anions (NO_3^- in the current case) encapsu-

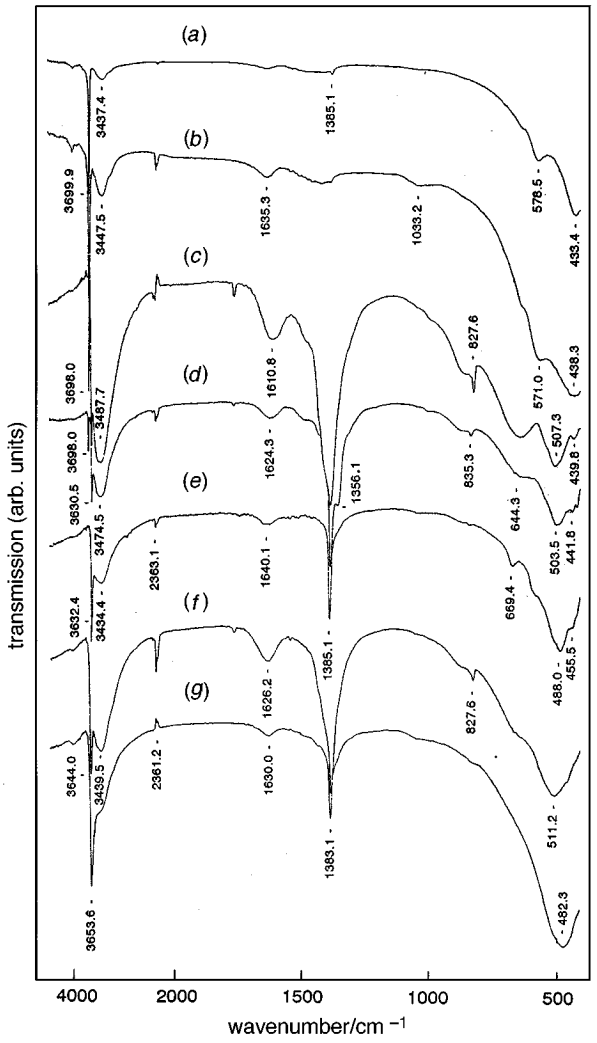

Fig. 1 FTIR spectra of the as-prepared precursor materials: (*a*) $Mg(OH)_2$ aged at 25 °C for 5 h, then dried at 60 °C overnight (25 + 60); (*b*) $Mg(OH)_2$ hydrothermally aged at 65 °C for 18 h, then dried at 60 °C for 18 h (65 + 60); (*c*) $Co(OH)_2$ aged at 25 °C for 5 h, then air-dried at 25 °C for 18 h (25 + 25); (*d*) $Co(OH)_2$ (25 + 60); (*e*) $Co(OH)_2$ (65 + 60); (*f*) MC1 (25 + 60); (*g*) MC2 (65 + 60)

lated *via* hydrogen bonding.[19–21] Water bending vibrations are also observable between 1611 and 1640 cm^{-1}. Anionic species such as NO_3^- and CO_3^{2-} (resulting from atmospheric CO_2 dissolution) can also be observed. In particular, the bands at 1356–1365 cm^{-1} (ν_3), 835–828 cm^{-1} (ν_2) and 669–644 cm^{-1} (ν_4) are assigned to the carbonate anion included in the material matrices while the sharp peaks at 1383–1385 cm^{-1} are assigned to the NO_3^- anion (ν_3 mode).[20,21] The absorption at 2361 cm^{-1} in all the spectra is due to the detection of CO_2 gas. Finally, peaks/bands at wavenumbers lower than 800 cm^{-1} can be attributed to metal–oxygen vibrations.[21,22]

For the monohydroxide $Mg(OH)_2$ (brucite), no NO_3^- inclusion is observable. In contrast to this, both NO_3^- and CO_3^{2-} absorptions are pronounced for $Co(OH)_2$ prepared at room-temperature. Nevertheless, CO_3^{2-} absorptions are reduced significantly in $Co(OH)_2$ which underwent hydrothermal treatment. Note that for the sample of $Co(OH)_2$ dried at 60 °C [Fig. 1(*d*)], two sharp peaks attributable to OH can be observed at 3698 and 3631 cm^{-1}. The former peak, with a value in close agreement with that for $Mg(OH)_2$ (3700 cm^{-1}), may suggest that a small portion of $Co(OH)_2$ has been transformed to a more brucite-like phase upon the heat treatment. The sharp peaks of OH vibrations at 3644 and 3654 cm^{-1} for MC1 and MC2 have intermediate values between those of $Mg(OH)_2$ and $Co(OH)_2$, indicating the formation of the double hydroxides of Mg–Co, *i.e.* mixed cations of both Mg and Co in the brucite-like structure. Based on the relative intensities of these peaks/bands, it is recognized that the water and carbonate anion contents in MC1 are much higher than in MC2.

As revealed by the elemental analyses (Table 1), MC1 has a Co/Mg atomic ratio of 4.37 and MC2 has a Co/Mg = 2.35. Clearly, the Co/Mg atomic ratio in the precipitates depends mainly on the ageing temperature. The above elemental analysis data are also in good agreement with the FTIR results. For example, the OH absorption at 3644 cm^{-1} (MC1; high Co/Mg) is closer to 3631–3632 cm^{-1} of $Co(OH)_2$ while the 3654 cm^{-1} (MC2; lower Co/Mg ratio) is nearer to 3700–3698 cm^{-1} of $Mg(OH)_2$. With the higher Mg content in the double hydroxide (MC2), the brucite-like sheet would generally be anticipated.[21] Furthermore, since the MC2 is hydrothermally treated at 60 °C for 18 h, higher crystallinity will also be expected. These two points are confirmed by the SEM morphological study reported in Fig. 2. Better crystallinity, greater grain sizes, more regular aggregates and flatter surfaces for MC2 are indeed observed. However, the calcination treatment at higher temperatures obviously led to considerable modifications in surface morphology, which will be addressed later.

NO_3^- and CO_3^{2-} anion exchange

When the MC1 and MC2 samples are immersed into the Na_2CO_3 solution, the NO_3^- group can be replaced by CO_3^{2-}, which is evidenced by the emergence of the CO_3^{2-} absorption at 1365 cm^{-1} (ν_3)[20,21] that is originally masked by the NO_3^- absorption (1383–1385 cm^{-1}) in most NO_3^--containing samples (Fig. 1). Based on the elemental analyses (Table 1), it is found that total negative charges borne by the anions of materials are well maintained before and after NO_3^-–CO_3^{2-} exchange, especially for the anion-rich case MC1. The observation here suggests the presence of a hydrotalcite-like phase in these catalyst precursors, taking the anion exchangeability into consideration.

The formation of a hydrotalcite-like phase is confirmed by the XRD investigation. As shown in Fig. 3 for the anion-rich sample MC1, the broad diffraction peaks are indeed characteristics of hydrotalcite-like compounds.[21,23,24] In the spectrum of MC2, however, this hydrotalcite feature is not observable; only pronounced brucite-like diffraction peaks can be seen. This observation is consistent with the low anion content found in the elemental analysis. The presence of the hydrotalcite-like phase in the MC1 samples indicates the formation of the trivalent cation (M^{3+}).[21,23,24] Owing to the presence of air atmosphere and common oxidation states of +2 and +3 for Co, a certain portion of the original Co^{2+} cations lose one of their $3d^7$ electrons and become Co^{3+} during the precipitate formation.[25] The anion inclusion in MC1 indeed reflects the above Co^{2+} oxidation process. When a Co^{2+} ion is oxidized to give Co^{3+}, the brucite-like sheet gains a positive charge. This positive gain can be balanced by an anion which possesses negative charge(s). Based on the elemental analysis data (Table 1), a deduced value of Co^{3+} $3d^6$:Co^{2+} $3d^7$ is *ca.* 23:77, or, atomic ratio Co^{3+}:($Co^{2+} + Mg^{2+}$) ≈ 19:81 in sample MC1 (and MC1C).

Nevertheless, it should be pointed out that both the hydrotalcite-like and brucite-like phases coexist in MC1, while the brucite-like phase is predominant in the MC2 samples (Fig. 3). In Fig. 4, the CO_3^{2-}/OH^- peak ratio of the MC1 series varies greatly with the NO_3^-–CO_3^{2-} exchange time whereas that of MC2 remains almost constant over the same time range. This indicates either a gradual loss of the hydrotalcite structure (*i.e.* a decrease in the inclusion capacity of CO_3^{2-}) or an increase in the brucite-like phase (*i.e.* an increase in the number of OH^- groups) for the prolonged anion-exchange experiments (> 60 min). In other words, MC1 is not as stable as MC2 with additional ageing in the basic aqueous solution.

Chemical/thermal stabilities and hydrothermal synthesis

In Fig. 5, the observed single endothermic peak of the $Mg(OH)_2$ sample corresponds to brucite decomposition, although this peak is shifted to higher temperature (420.0 °C) in the sample subjected to hydrothermal treatment at 60 °C. Compared to this, the decomposition occurs at a much lower temperature of 188.9 or 188.1 °C (Fig. 5) for the $Co(OH)_2$ samples without hydrothermal treatment. Interestingly, this peak shifts to 206.4 and 267.0 °C for the sample which underwent hydrothermal ageing. The latter (267.0 °C) can be attributed to a more brucite-like phase since the anion population (Fig. 1) is significantly lower for this sample. The small peaks located at low temperatures (166.7 and 170.2 °C) can be assigned to the removal of the water molecules trapped in the interlayer spacing between the brucite-like sheets, *i.e.* the gallery water molecules,[21,23–27] because these cobalt hydroxides also show hydrotalcite-like features in their XRD spectra.

Table 1 Preparation conditions and elemental analysis results for MC1, MC2 and their CO_3^{2-}-exchanged samples

sample	initial Co:Mg ratio	precipitation pH	precipitating atmosphere	ageing/drying temperature /°C	elemental analysis						
					CO_3^{2-} (mass%)	NO_3^- (mass%)	NO_3^-/CO_3^{2-} (mol ratio)	Mg (mass%)	Co (mass%)	Co/Mg (mol ratio)	Co^{3+}/Co^{2+} (mol ratio)
MC1	1	9.5	air	25;60	1.25	7.69	5.96	4.06	42.96	4.37	23:77
MC2	1	9.5	air	65;60	1.30	0.40	0.30	7.60	43.44	2.35	—
MC1C[a]	1	9.5	air	25;60	5.35	0	0	3.90	45.21	4.79	23:77
MC2C[a]	1	9.5	air	65;60	2.45	0.35	0.14	7.39	44.10	2.46	—

[a]MC1 or MC2 impregnated in a 0.5 mol dm^{-3} Na_2CO_3 aqueous solution for 1 h under stirring at room temperature.

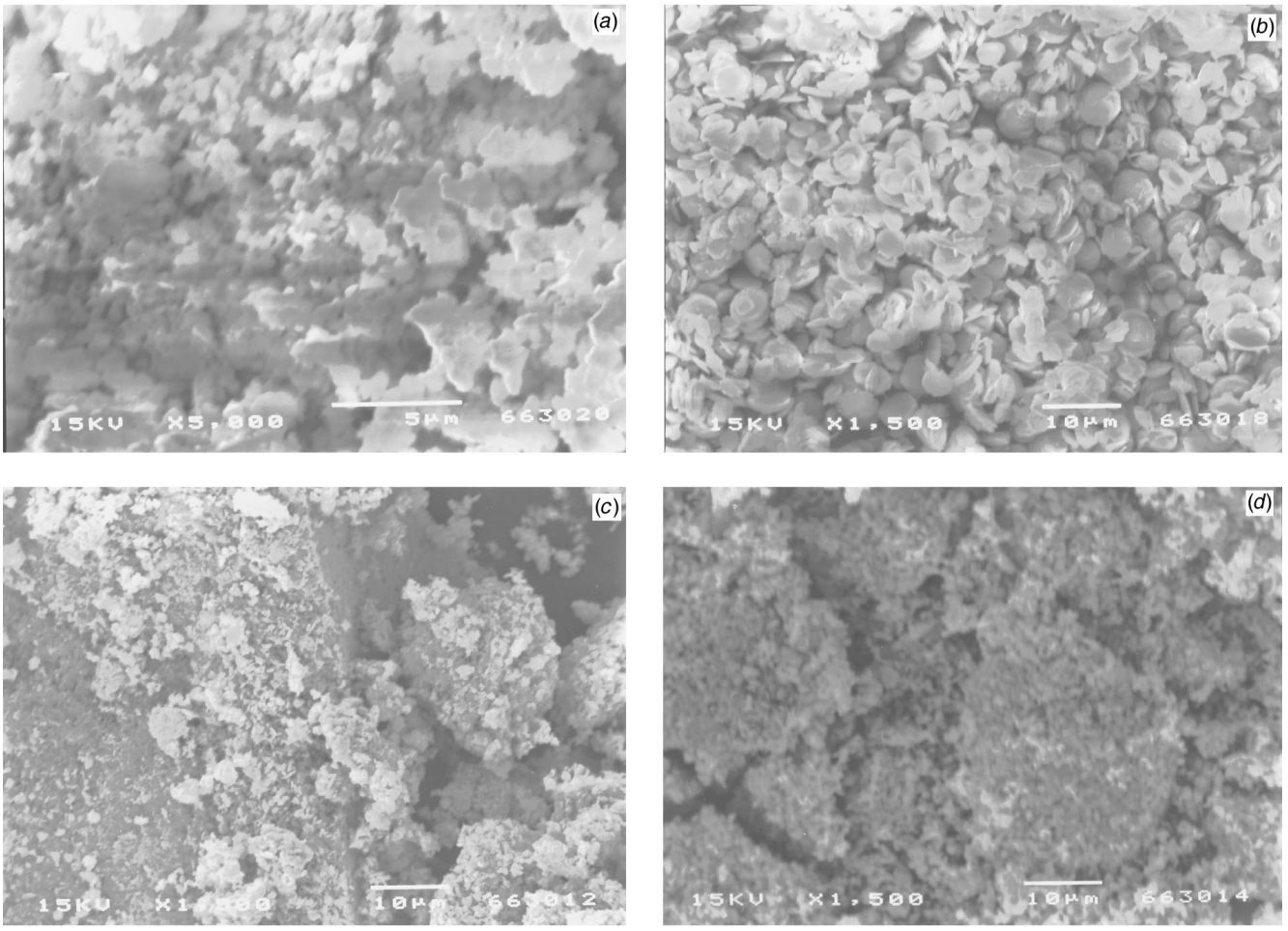

Fig. 2 SEM images of: (*a*) as-prepared MC1; (*b*) as-prepared MC2; (*c*) MC1 after calcination at 350 °C for 2 h; (*d*) MC2 after calcination at 350 °C for 2 h

In line with the XRD results (Fig. 3), the DSC plot of MC1 reported in Fig. 6 also suggests the formation of a hydrotalcite-like phase. The endothermic peak at 113.1 °C can be assigned to gallery water molecule depletion,[21,23–27] since water adsorption/desorption is reversible at this temperature. The main peak at 229.6 °C, however, is attributable to the collapse of the hydrotalcite-like phase.[21,23–27] Based on the DSC results for hydrothermally treated $Co(OH)_2$, the high-temperature peak of 282.7 °C can be ascribed to the decomposition of the hydroxide phase remaining in MC1, which was detected in the XRD study. Although no direct evidence is given, the tiny peak at 192.8 °C may be due to the desorption of surface adsorbed water prior to the collapse of the hydrotalcite framework, using a similar explanation in other hydrotalcite compounds.[26]

For hydrothermally heated samples MC2, the thermal behaviour is substantially different. For example, the gallery water desorption at low temperatures is barely observed. The decomposition temperatures, on the other hand, have been shifted to higher values, owing to the low Co/Mg ratio in MC2. Therefore, the thermal behaviour of MC2 can be described as being between the hydrothermally treated $Mg(OH)_2$ and $Co(OH)_2$ (Fig. 5), noting that with the prolonged thermal drying, endothermic peaks for MC2 move further to the high-temperature side.

Calcination and surface areas

As was addressed in the previous section, MC2 with the high Mg content is more thermally stable than MC1. This observation is further reflected in the FTIR spectra of Fig. 7 for calcined MC1 and MC2 samples. For the as-prepared MC1 and MC2, metal–oxygen vibration absorptions are located at 511 and 482 cm^{-1} respectively. With increasing calcination temperatures, the spectrum evolution reveals the formation of mixed metal oxides, *i.e.* a spinel-type phase.[22] The doublet peaks for the high-temperature calcined samples are similar to those reported in the literature for pure Co_3O_4 (661 and 568 cm^{-1}).[28,29] In the current study, doublet peaks of monohydroxide $Co(OH)_2$ calcined at 500 °C for 2 h are located at 664 and 567 cm^{-1}, indicating the formation of a Co_3O_4 phase. Note that the wavenumber of the first peak of MC1 (652 cm^{-1}) is higher than that of MC2 (646 cm^{-1}), *i.e.* with increasing Mg content, the peak shifts towards the lower wavenumber region. The departure from 664 cm^{-1} (of Co_3O_4) can be attributed to the inclusion of Mg (more M^{2+} species) into the Co_3O_4 spinel phase. From the decoupling temperature of the doublet peaks, it can be concluded that MC2 is thermally more stable. The decomposition of the catalyst precursors is also reflected in the XRD spectra of Fig. 3(*c*) and (*d*) (at 350 °C), indicating that the resultant oxides are largely amorphous, although a weak spinel-type feature can be observed in Fig. 3(*c*).[30]

Fig. 8 shows the results of BET measurements for the above two calcined sample series. When the hydroxide/hydrotalcite phases are converted to metal oxides, the surface area varies substantially. For example, the surface area of MC1 reaches a maximum at 250 °C and later declines at higher temperatures since it is Co-rich and decomposes readily. For the MC2 series, however, the surface area does not reach a maximum until 300 °C, since it is more stable to sustained thermal treatment. In both cases, the maximum surface area is obtained when the

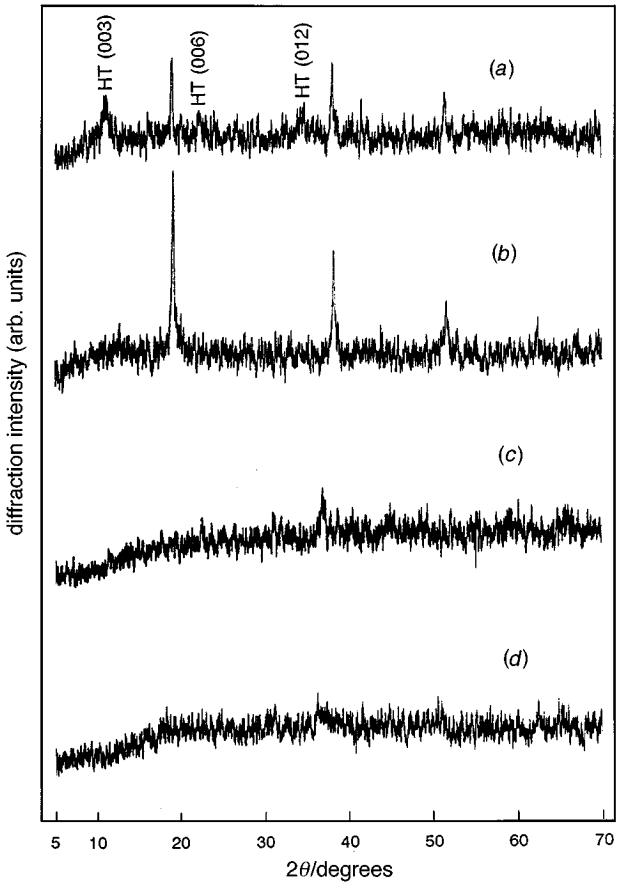

Fig. 3 XRD spectra of: (*a*) as-prepared MC1 (HT indicates the hydrotalcite phase); (*b*) as-prepared MC2; (*c*) MC1 calcined at 350 °C for 2 h; (*d*) MC2 calcined at 350 °C for 2 h

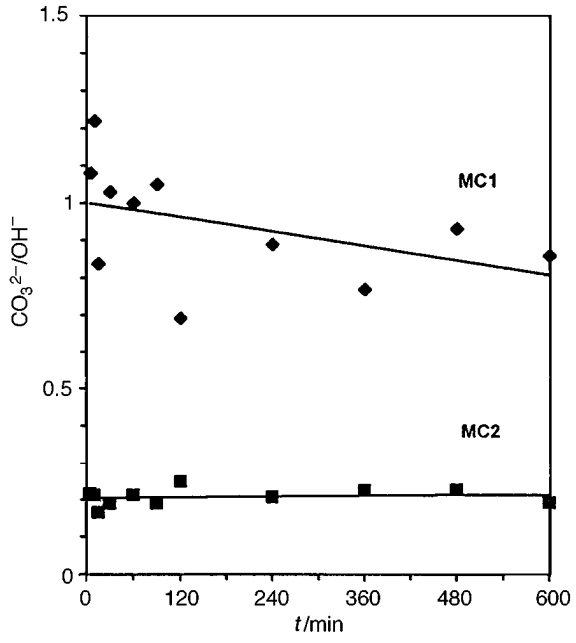

Fig. 4 FTIR peak ratio of CO_3^{2-}/OH^- *vs.* NO_3^-–CO_3^{2-} exchange time; the FTIR peak height of CO_3^{2-} is based on the absorption at 1365 cm^{-1} (ν_3), and the height of OH^- is measured from the sharpest/strongest peak assigned for the double hydroxide framework

hydroxide/hydrotalcite framework collapses, *i.e.* it occurs at metal oxide formation temperatures. The decrease in surface area at higher calcination temperatures can be explained by oxides grain growth.

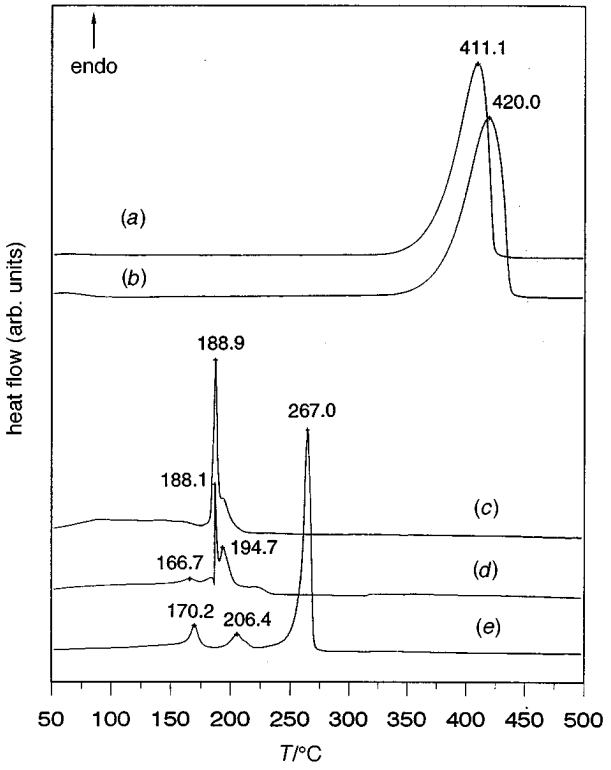

Fig. 5 DSC plots of the monohydroxide samples: (*a*) $Mg(OH)_2$ (25+60); (*b*) $Mg(OH)_2$ (65+60); (*c*) $Co(OH)_2$ (25+25); (*d*) $Co(OH)_2$ (25+60); (*e*) $Co(OH)_2$ (65+60)

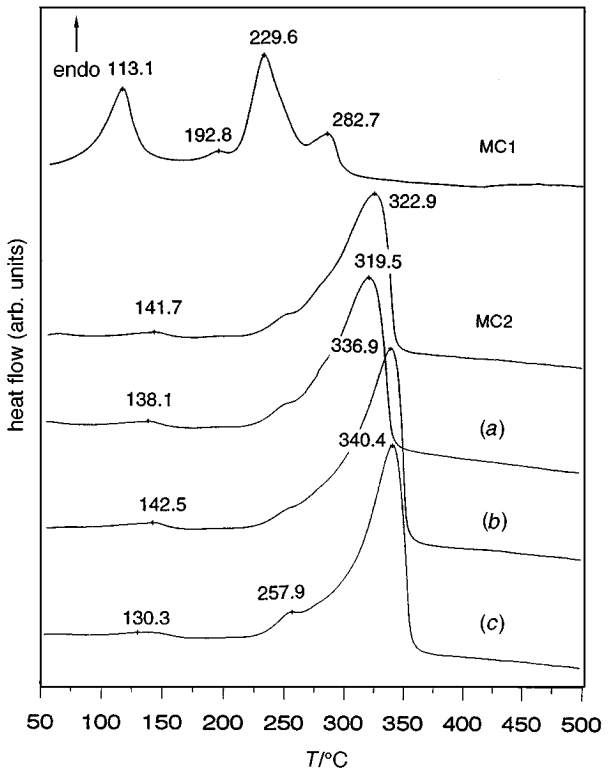

Fig. 6 DSC plots of the as-prepared double-hydroxide samples MC1 (25+60), MC2 (65+60), and prolonged heat-dried MC2 (65+60): (*a*) MC2 with a total drying time of 42 h at 60 °C (65+60/42h); (*b*) MC2 (65+60/66h); (*c*) MC2 (65+60/114h)

Catalytic performances

In the current investigation, all the Mg–Co oxides studied exhibit reasonable catalytic activities for N_2O decomposition. As shown in Fig. 9, MC1 and MC2 give a noticeable activity

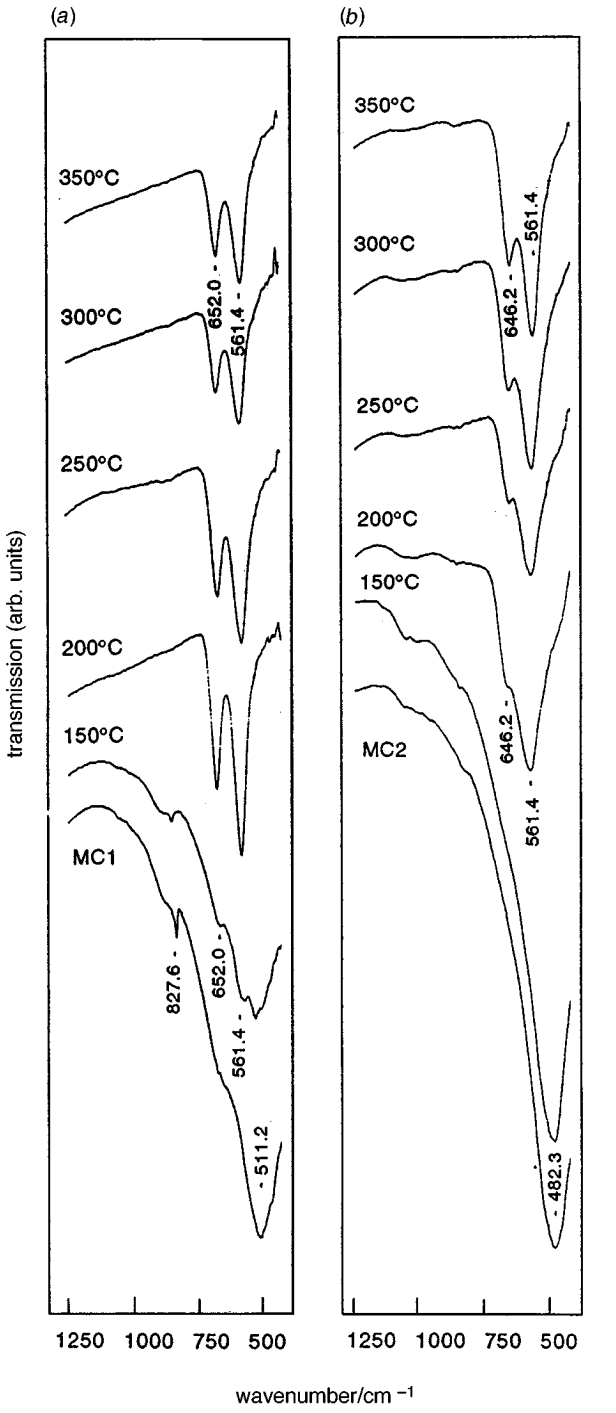

Fig. 7 FTIR spectra of calcined MC1 (*a*) and MC2 (*b*) sample series at different elevated temperatures

at temperatures as low as 250–275 °C and 275–300 °C respectively. Under these experimental conditions, approximately 6 moles of N_2O per kg of the hydroxide/hydrotalcite can be decomposed at 350 °C within 1 h, which is comparable to some of the most active catalysts reported so far.[1–18] It is recognized that the activity difference between MC1 and MC2 is not due solely to surface area variations. For example, the surface area of MC2 is *ca.* 40% higher than that of MC1 after calcination (Fig. 8), whereas MC2 is *ca.* 200% more active than MC1 at 350 °C (Fig. 9). Since the atomic mass of Mg is much lower than that of Co, the total amount of metal cations in the MC2 catalyst is higher than that in MC1. It is therefore suggested that the higher catalytic activity observed for MC2 is attributable to the larger number active sites formed by Mg–O–Co with an appropriate atomic ratio of Mg/Co. Apparently, the

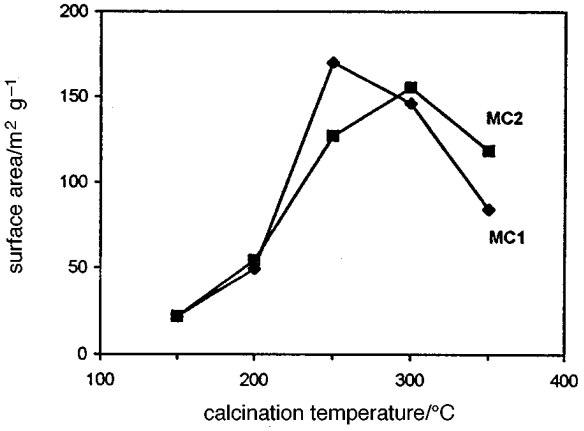

Fig. 8 BET measurements for the calcined MC1 and MC2 sample series; two sets of data are averaged for each sample series

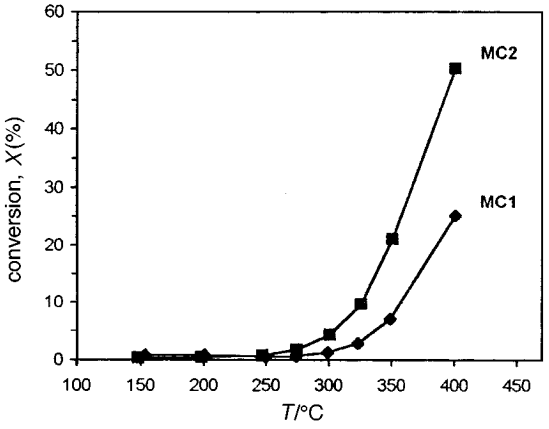

Fig. 9 Catalytic activity [X, eqn. (1)] evaluation for the MC1 and MC2 catalysts; prior to the catalytic test, as-prepared MC1 or MC2 was decomposed *in situ* under the flow of the reaction mixture at 350 °C

optimization of the Mg/Co ratio and other processing parameters are needed in further study.

Conclusions

In summary, binary metal oxide catalysts of Mg–Co have been synthesized from Mg–Co hydroxide/hydrotalcite precursors for low-temperature N_2O decomposition. Higher Mg contents and higher crystallinity are observed in the hydrothermally treated precursor. With the anion-exchange method and XRD, a hydrotalcite-like phase is also found due to a partial oxidation of Co^{2+} to Co^{3+}. The catalyst prepared from the hydrothermally treated precursor is more active and stable compared with the one aged at room temperature. All precursor materials give amorphous Mg–Co oxides after thermal decomposition. The resultant oxides have shown high catalytic activity for N_2O decomposition. At 350 °C, approximately 6 moles of N_2O per kg of precursor hydroxide/hydrotalcite can be decomposed within 1 h.

The authors gratefully acknowledge the research funding (RP3950619) supported by the National University of Singapore for the experimental study of catalytic materials. H. C. Z. would also like to thank Dr. T. A. Koch and Dr. J. C. Wu of E. I. DuPont de Nemours & Co., Inc., USA, for the recommendation of this research topic.

References

1 M. H. Thiemans and W. C. Trogler, *Science*, 1991, **251**, 932.
2 Y. Li and J. N. Armor, *Appl. Catal. B*, 1992, **1**, L21; 1993, **3**, 55; *US Pat.*, 1992, 5 149 512; 1992, 5 171 553.

3 A. P. Kinzig and R. H. Socolow, *Phys. Today*, 1994, **47**, 24.
4 H. C. Zeng, J. Lin, W. K. Teo, J. C. Wu and K. L. Tan, *J. Mater. Res.*, 1995, **10**, 545.
5 H. C. Zeng and M. Qian, *J. Mater. Chem.*, 1996, **6**, 435.
6 Y-F. Chang, J. G. McCarty, E. D. Wachsman and V. L. Wong, *Appl. Catal. B*, 1994, **4**, 283.
7 G. D. Lei, B. J. Adelman, J. Sarkany and W. M. H. Sachtler, *Appl. Catal. B*, 1995, **5**, 245.
8 L. M. Aparicio and J. A. Dumesic, *J. Mol. Catal.*, 1989, **49**, 205.
9 J. Valyon, W. S. Millman and W. K. Hall, *Catal. Lett.*, 1994, **24**, 215.
10 G. I. Panov, V. I. Sobolev and A. S. Kharitonov, *J. Mol. Catal.*, 1990, **61**, 85.
11 B. W. Riley and J. R. Richmond, *Catal. Today*, 1993, **17**, 277.
12 P. Pomonis, D. Vatts, A. Lycourghiotis and C. Kordulis, *J. Chem. Soc., Faraday Trans. 1*, 1985, **81**, 2043.
13 A. K. Ladavos and P. J. Pomonis, *Appl. Catal. B*, 1993, **2**, 27.
14 R. Sundararajan and V. Srinivasan, *Appl. Catal.*, 1991, **73**, 165.
15 S. L. Raj, B. Viswanathan and V. Srinivasan, *J. Catal.*, 1982, **75**, 185.
16 D. D. Eley, A. H. Klepping and P. B. Moore, *J. Chem. Soc., Faraday Trans. 1*, 1985, **81**, 2981.
17 S. Kannan and C. S. Swamy, *Appl. Catal. B*, 1994, **3**, 109.
18 X. Y. Pang, H. C. Zeng, J. C. Wu and K. Li, *Appl. Catal. B*, 1996, **9**, 149.
19 F. Trifiro, A. Vaccari and G. D. Piero, in *Characterization of Porous Solids*, ed. K. K. Unger, Elsevier Science, Amsterdam, 1988, p. 571.
20 E. C. Karuissink, L. L. Van Reijen and J. R. H. Ross, *J. Chem. Soc., Faraday Trans. 1*, 1981, **77**, 649.
21 F. Cavani, F. Trifiro and A. Vaccari, *Catal. Today*, 1991, **11**, 173.
22 G. Busca, F. Trifiro and A. Vaccari, *Langmuir*, 1990, **6**, 1440.
23 W. T. Reichle, *Solid State Ionics*, 1986, **22**, 135.
24 K. A. Carrado, A. Kostapapas and S. L. Suib, *Solid State Ionics*, 1988, **26**, 77.
25 H. C. Zeng, M. Qian and Z. P. Xu, unpublished work.
26 S. K. Yun and T. J. Pinnavaia, *Chem. Mater.*, 1995, **7**, 348.
27 F. Rey, V. Fornes and J. M. Rojo, *J. Chem. Soc., Faraday Trans.*, 1992, **88**, 2233.
28 H. D. Lutz and M. Feher, *Spectrochim. Acta, Part A*, 1971, **27**, 357.
29 J. Preudhomme and P. Tarte, *Spectrochim. Acta, Part A*, 1971, **27**, 1817.
30 G. Fornasari, S. Gusi, F. Trifiro and A. Vaccari, *Ind. Eng. Chem. Res.*, 1987, **26**, 1500.

Paper 6/07627K; *Received* 8*th November*, 1996